PHYSICAL REVIEW A VOLUME 25, NUMBER 6 JUNE 1982

K-shell ionization cross sections for Ti, Cr, Co, Ni, Cu, and Zn targets induced by protons in the energy range 300–2400 keV

M. D. Brown, D. G. Simons, D. J. Land, and J. G. Brennan*
Naval Surface Weapons Center, White Oak, Silver Spring, Maryland 20910
(Received 2 November 1981)

Absolute K-shell x-ray-production cross sections have been measured for thin-foil targets of Ti, Cr, Co, Ni, Cu, and Zn at incident proton beam energies from 300 to 2400 keV. Particular care was necessary in the control of experimental conditions in order to determine the x-ray-production cross sections with high precision (~5%). The x-ray-production cross sections were determined from x-ray yields normalized to simultaneous measurements of particle scattering yields at 90°. The values of K-shell vacancy-production cross sections were determined to range from 0.133 b for 300-keV protons on Zn to 1230 b for 2400-keV protons on Ti. The overall agreement of these total cross sections with recent data obtained by other workers generally is to within 10% and frequently is to within the 5% accuracy of our results. The K-shell ionization cross sections inferred from these results are compared with the predictions of energy-loss Coulomb-deflection perturbed-stationary-state relativistic theory which reproduces the data with good accuracy. In addition, these results also show good agreement when compared with a more fundamental formulation based on perturbed-stationary-state theory.

I. INTRODUCTION

The direct Coulomb ionization of an inner-shell electron by a swiftly moving charged particle is a fundamental problem in atomic collision physics. K-shell vacancy production by energetic protons has been the subject of many theoretical and experimental investigations. In recent years the experimental effort has been directed to the measurement of cross sections with increased accuracy to establish a data base for quantitative proton-induced x-ray emission analysis including quantitative trace element analysis, stoichiometry, and depth concentration determination, and for other applied studies. In addition, absolute cross sections provide a good test of the predictive capability of the present theoretical formalisms.

The present work was undertaken to determine a few inner-shell ionization cross sections with high precision. Total cross sections for K-shell x-ray production for incident proton beams with selected energies in the range from 0.3 to 2.4 MeV were measured in thin elemental targets of Ti, Cr, Co, Ni, Cu, and Zn. In order to limit the experimental error to approximately 5%, special care was required in the experimental design and implementation.

Through the years many measurements of inner-shell ionization have been made with varying degrees of accuracy. A recent summary[1] of these data shows in many cases a wide variance among the reported values. However, two sets of accurate measurements[2,3] (10% or better) were presented at the 1979 Workshop on Inner-Shell Ionization by Light Ions. These measurements cover a similar range of target atomic number and proton energy as the present study reported here. These data agree with each other generally to within the quoted error. The present measurements, which are estimated to have an error of about 5%, are in close agreement with these two measurements. It is hoped that our data along with the other high-accuracy measurements can serve as a solid data base for applied studies using ion-beam analysis.

This paper is organized into five sections. In Sec. II which deals with experimental procedures, the design of the experimental apparatus and the methods employed to reduce uncertainties in the data are given. In addition, the analysis of the data is explained, and a detailed estimate of the sources of error is discussed. In Sec. III the values of the measured cross sections are reported, and direct comparisons with other measurements are discussed. In Sec. IV, which deals with theoretical considerations, a brief overview of the theoretical approaches to calculating inner-shell ionization cross sections is given. Comparisons of our data are made with two theoretical formalisms. Predic-

tions of the energy-loss Coulomb-deflection perturbed-stationary-state-relativistic (ECPSSR) theory[4] are found to reproduce the present measurements very closely. Results of a more fundamental approach[5] formulated within the context of perturbed-stationary-state theory[6] also show good agreement. In Sec. V a summary of this work is given and conclusions drawn.

II. EXPERIMENTAL PROCEDURES

In this study the K-shell ionization cross sections are inferred from measurements of the x-ray-production cross sections and tabulated values of the fluorescence yields.[7] The x-ray-production cross section is obtained by normalizing the x-ray yield to the scattered particle yield. These yields are determined by simultaneously measuring the x rays and scattered particles for incident monoenergetic protons on thin-foil targets. This procedure[2,3,8] has become quite standard for precision measurements of total x-ray cross sections because it eliminates the need for accurate determination of target thicknesses and beam currents. In this work it is assumed that the particle scattering is purely Rutherford. This assumption was experimentally supported since the ratio of the counting rates between the two particle detectors (see description below) remained constant to within counting statistics over the energy range of this investigation.

The experimental setup is shown schematically in Fig. 1. The x-ray and particle detectors were mounted at 90° to the incident beam. Apertures were mounted in front of these detectors to eliminate detector edge effects. Aperture sizes and target-to-detector distances were chosen to allow accurate solid-angle measurements. Cleaning apertures were also placed between the target and the detector apertures to restrict the field of view of the detector in order to minimize spurious events. Scattered particles were also counted simultaneously with an annular surface-barrier monitor detector at an average scattering angle of 178.4° to the incident beam. The beam was defined through two 1-mm-diameter apertures 82.5 cm apart which gave an angular divergence of approximately 1.2 mrad. A 2.5-mm cleaning aperture was placed between these two beam-defining apertures to minimize slit-edge scattering.

The total K-shell vacancy-production cross section determined by the procedures used here is given by

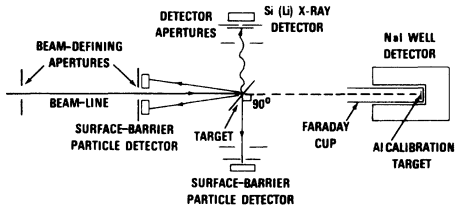

FIG. 1. Experimental arrangement use for the present measurements of x-ray-production cross sections.

$$\sigma_v(E)=\frac{N_x(d\sigma^R/d\Omega)(\theta,E)d\Omega_p}{N_p\omega_k\xi_x d\Omega_x/4\pi}\ , \tag{1}$$

where N_x and N_p are the number of x rays and particles counted; $(d\sigma^R/d\Omega)(\theta,E)$ is the Rutherford scattering cross section calculated at the particle scattering angle θ and energy E; $d\Omega_P$ and $d\Omega_x$ are the solid angles subtended by the particle and x-ray detectors, respectively; ω_k is the target fluorescent yield; and ξ_x is the x-ray detector efficiency for the $K\alpha\beta$ x rays. The accuracy of the measurement for the total cross section thus depends on the accuracy of the determination of each of the above parameters. We shall discuss how each of these parameters was determined, their accuracy, and any other corrections to the data which went into the final determination of σ_v.

A. Counting statistics

As the incident proton energy is increased, the Rutherford scattering cross section decreases, and the x-ray production cross section increases. In order to ensure that the x-ray and scattered particle counting rates were comparable at each energy, the solid angle of the particle detector was changed when necessary. In all cases counts were accumulated to ensure that the error introduced in the counting statistics was $\leq 1\%$.

B. X-ray detector solid angle

The x-ray detector solid angle was measured two ways, geometrically and with a calibrated radioactive source. Agreement to within experimental accuracy was required between these two methods before proceeding with the experiment. For the solid-angle measurement determined using a radioactive source we employed an ^{55}Fe source whose

intensity was calibrated by the National Bureau of Standards (NBS) to an accuracy of 1.8%. In order to determine the x-ray detector solid angle from the detected x-ray intensity, corrections for detector efficiency were necessary. Good agreement between the geometrical solid angle and that measured using the radioactive source was obtained when the source strength was calculated from the recently determined ^{55}Fe half-life of 1006.7 ± 2.5 days.[9] As an added check on the source intensity, this source was recalibrated by the NBS after the solid-angle measurements were completed and the original calibration was confirmed. An x-ray detector solid angle of 6.48×10^{-4} sr was determined from these measurements.

The solid-angle measurement also provided a good basis for determining detector efficiencies. The x-ray detector efficiency was calculated by including x-ray absorption by the detector dead layer (1000 Å), the gold layer on the front surface (200 Å), and the Be window (0.025 mm). The x-ray detector is a Si (Li) detector with a 190-eV resolution for ^{55}Fe x rays and has a sensitive depth of 5.3 mm. A 0.1-mm polyethylene absorber was placed in front of this detector to prevent scattered protons from entering the detector and causing radiation damage. The absorptions of the polyethylene absorber were measured for ^{55}Fe and ^{54}Mn x rays and found to agree with the calculated values to better than 1%. The good agreement of the solid angle measured using the detector efficiency determined for ^{55}Fe x rays with the geometrical solid angle gives support to the absorber thicknesses and mass-absorption coefficients[10] used. The efficiencies determined for the weighted average of the K x rays[11] of the targets used in this experiment ranged from 0.752 for titanium to 0.958 for zinc and are given in Table I. These efficiencies include the effects of the 0.1-mm polyethylene absorber whose density was determined in a separate measurement.

C. Particle-detector solid angles

The particle detectors are Si surface-barrier detectors with typical resolutions of 15–20 keV. Two different α sources were used for the solid-angle determinations, ^{241}Am and ^{148}Gd. Both sources were calibrated by the NBS to accuracies of 1.0% and 1.7%, respectively. Agreement in the measurements of the solid angle determined using each of these sources and determined geometrically was required. During the initial calibration, the solid-angle measurements of the 90° detector using the ^{148}Gd source was consistently 2–3 % lower than the geometrical and ^{241}Am values (which were in agreement). This difference was eliminated when the detector was replaced with a new one. The two solid angles used for the 90° detector were 1.74×10^{-4} and 6.96×10^{-6} sr. The smaller solid angle was used at lower-beam energies to reduce the particle counting rates, in order to keep a balance between the x-ray and particle counting rates. Particle-detector efficiencies of 100% were assumed.

TABLE I. Detector efficiencies employed in the data reduction and target thicknesses used during the experimental investigation. Total detector efficiencies listed include the absorption of 0.1-mm polyethylene and are weighted by the $K\alpha,\beta$ intensities. Target thicknesses were measured using the Rutherford backscatter (RBS) of 2-MeV ^{4}He ions. Except for the copper target, which was self-supporting, all targets were evaporated on ≈ 2.5 μg/cm^2 of carbon.

Target element	Detector efficiency[a,b]	Thickness (Å) Proton energy range 300–600 keV	700–2400 keV
Ti	0.752	590	590
Cr	0.850	600	600
Co	0.920	550	610
Ni	0.936	520	600
Cu	0.951	530	650
Zn	0.958	1050	400

[a]The absorption coefficients were taken from Ref. 10.
[b]The intensities of the $K\alpha,\beta$ x rays were taken from Ref. 11.

The annular monitor detector is a surface-barrier detector with a 4.0-mm hole in the center through which the beam was directed. One of the 1-mm beam-defining apertures was placed directly upstream of this detector. In order to prevent slit-edge scattered particles from striking the inner edge of the detector annulus, a 2.0-mm i.d. aluminum tube was placed through the detector hole. The annular particle detector was determined to have a solid angle of 2.80×10^{-3} sr as measured by the ^{241}Am and ^{148}Gd sources and geometrically.

D. Rutherford scattering cross section

The precision measurement of the total K-shell vacancy-production cross section using the present technique requires accurate values for the particle scattering angle θ and beam energy E, from which the Rutherford scattering cross section $d\sigma^R/d\Omega$ for the normalization detector is determined (see Fig. 1). At a 90° scattering angle for the normalization detector, a variation in the scattering angle of 1° changes the Rutherford scattering cross section and hence the K-shell vacancy-production cross section by 3%. The scattering angle was determined by normalizing the particle counting rate in the 90° detector to the counting rate obtained in the annular detector where the Rutherford scattering cross section is less sensitive to variations in the scattering angle. For the annular particle detector mounted at a scattering angle of 178.4°, a variation in the scattering angle of 1° changes the Rutherford scattering cross section by 0.3%. The scattering angle of the normalization detector was determined to be $89.6°\pm0.5°$ by this procedure.

Accurate determination of the beam energy is necessary because of the combined effects of the E^{-2} dependence of the particle yield N_p and the E^2 to E^4 dependence of the x-ray yield N_x. From Eq. (1) we see that σ_v depends upon the ratio of these two yields N_x/N_p, which can vary as strongly as E^6 at the lowest energies. The beam energy was determined to within 1 keV by calibrating the accelerator using the ^{27}Al$(p,\gamma)^{28}$Si resonance reaction at 991.88 keV. The beam was bent through a 90° analyzing magnet where the magnetic field was measured by a nuclear magnetic resonance (NMR) probe. The NMR system was used to establish the beam energy over the entire energy range. Voltage fluctuations at the terminal were kept to a minimum by using a constant current charging supply and a corona discharge system controlled by a combination of terminal capacitance pick-off and exit-slit feedback. As observed on the capacitance pick off, the measured voltage accuracy of 1 keV obtained at the calibration energy was maintained throughout the entire energy range studied here. Thus, at 300 keV there is an error in σ_v of about 2% as a result of the fluctuations in terminal voltage. This error falls off to about 0.2% at the highest energy used (2400 keV).

E. Spectral corrections

The particle and x-ray spectra were each analyzed with a single-channel analyzer and counted on high-speed scalers. Counting rates were kept sufficiently low so that rejection of pile-up pulses was minimized. However, analysis of x-ray spectra from ^{55}Fe and particle spectra from self-supporting thin targets showed low-energy portions of the spectra which are not recorded in the single-channel analyzers. To obtain N_p and N_x, the SCA counts were thus corrected to include these lower-energy pulses which were attributed primarily to incomplete charge collection. These corrections, obtained from multichannel-analyzer (MCA) spectral measurements, increase the single-channel analyzer count for the particle detector by 4.75% and for the x-ray detector by 2.50%.

Continuous MCA monitoring of the particle spectra also allowed counting corrections to be made for contributions from the buildup of C and O on the target surfaces or from the C foil substrates of the films studied. Actually, the detector resolutions were sufficient so that no such corrections were necessary except for the 300-keV measurements on Cr.

F. Fluorescence yield

The values of the fluorescence yield ω_k were taken from the best-fit values of Bambynek *et al.*[7] No corrections or errors in ω_k were included in our final values of σ_v.

G. Target thickness

The values of the total cross sections were corrected to reflect their value for the quoted proton energy at the center of the target foil. Foil

thicknesses were obtained by Rutherford backscatter measurements with 2.0-MeV ^{4}He scattered into the annular particle detector at 178.4°. Standard thin-foil analysis was employed using the ^{4}He stopping powers of Ziegler.[12] The targets and their thicknesses are given in Table I. In making these corrections we assumed a local energy dependence of the cross section of $\sigma_v = AE^p$. The value of p was obtained from calculation of σ_v using the ECPSSR theory.[4] In addition, the energy dependence of the Rutherford scattering cross section was also taken into account. A correction factor of

$$1+\frac{2+p}{2}\frac{\Delta x}{E}\frac{dE}{dx}$$

is required, where Δx is the foil thickness, E the incident beam energy, and dE/dx the proton stopping power at energy E. A small carbon buildup on the targets was observed, but its thickness was always such that energy-loss corrections could be neglected. For 300-keV protons on Zn a correction factor of 1.22 was necessary. This value is accurate to about 2% and is the largest correction factor encountered. As the beam energy is increased, the correction factors decrease to values of about 1.005 at the highest energies.

H. Errors

The major sources of error are discussed above. A detailed analysis of the magnitude for each source of error was made. The total estimated error accumulated in quadrature is approximately 5%. The value of the errors from these analyses are listed in Table II. It should be noted that, because of beam-energy and energy-loss considerations, the accumulated error decreases as the beam energy increases from 300 keV to 2.4 MeV.

TABLE II. Sources of uncertainty in the measured cross sections at 300 keV and 2 MeV. These errors are approximately the same for all targets. Worst-case values are given here. Total estimated error is accumulated in quadrature.

Error source	Beam energy 300 keV (%)	Beam energy 2 MeV (%)
Counting statistics	1	1
Solid angles		
X-ray detector	2	2
Particle detector	2	2
X-ray detector	2	2
Beam energy	2	0.2
Rutherford cross section (scattering angle)	3	3
Energy loss through target	2	0.5
Total estimated error	5.5	4.7

III. RESULTS AND DISCUSSION

Total K-shell vacancy-production cross sections for protons on Ti, Cr, Co, Ni, Cu, and Zn were measured at particle energies from 300 to 2400 keV. The resulting numerical values of the cross sections in barns are tabulated in Table III. The fluorescent yields[7] used in the data reduction are also listed. These results are compared directly to recent experimental data of similar accuracy by other investigators. Three data sets[2,3,13] were chosen such that extensive comparisons could be made with our data. The data of Ref. 13 have been adjusted to correspond with the energies of our measurements. In this manner we hoped to determine with additional confidence the overall accuracy of these investigations. From the tabulated data in Table III it is noted that the cross sections vary over four orders of magnitude. For a more sensitive data comparison the ionization cross section measured in other studies is divided by the cross section determined in this investigation. This method allows a detailed data comparison over the entire proton energy range. The results of this comparison are plotted against the energy of the bombarding proton beam for each target and are shown in Fig. 2. The agreement among each of these three data sets with our data is seen to be very good. In fact, the agreement is almost always to within the quoted error and generally is to within the 5% accuracy of our results.

However, the comparisons with each of the different data sets shows some discrepancies. In particular, the results of this investigation tend to be systematically larger by a few percent than those reported in the other works. However, there is no easily identifiable pattern which holds from element to element. Indeed, the comparison for copper shows an excellent agreement for all the data sets. In the case of nickel the two data sets are approximately 10% below our results over the entire proton energy range. This difference would indicate that our data set for nickel is too large or

TABLE III. Total K-shell vacancy-production cross sections induced by energetic protons. Values of the cross sections are given in barns and the proton energies are given in keV. Errors in the values of the cross sections are of the order of 5%.

E_p (keV)	Ti($Z=22$) $\omega_k=0.219$[a]	Cr($Z=24$) $\omega_k=0.282$	Co($Z=27$) $\omega_k=0.381$	Ni($Z=28$) $\omega_k=0.414$	Cu($Z=29$) $\omega_k=0.445$	Zn($Z=30$) $\omega_k=0.479$
300	5.48	2.26	0.533	0.347	0.212	0.133
400	15.4	6.08	1.63	1.07	0.710	0.466
500	32.4	13.7	3.69	2.43	1.70	1.09
600	57.5	24.7	6.92	4.75	3.24	2.12
700	86.9	37.4	11.4	7.92	5.18	3.53
800	131	56.3	17.0	12.4	8.25	5.59
1000	223	101	32.9	23.4	16.3	11.4
1200	350	159	54.6	39.7	27.4	19.3
1400	491	226	80.1	58.2	41.8	29.8
1600	631	300	113	80.9	59.3	42.4
1800	788	388	149	106	78.7	58.1
2000	949	450	179	134	95.8	72.5
2200	1080	539	220	163	120	89.4
2300			236	178	129	103
2400	1230	631	257	192	142	108

[a]The fluorescence yields are the fitted values given in Ref. 7.

the other data sets are too small, or both. When our nickel data are compared with theory (see Figs. 3 and 4 and Sec. IV) there is no corresponding 10% discrepancy. The largest variations in these data comparisons occur at the lowest proton energies where the cross sections depend most sensitively on the beam energy and the target thickness. The differences at low energies are largest for Ti and Zn. At the lowest proton energies the cross-section ratios plotted in Fig. 2 increase for Ti, Co, and Zn and decrease for Cr. Again, when our data are compared with theory (see Figs. 3 and 4) no discrepancy of this kind exists. In particular, the largest ratios are not seen. Clearly additional measurements in the low-energy range are desirable to help resolve these discrepancies.

IV. THEORETICAL CONSIDERATIONS

There have been many theoretical approaches to the problem of calculating the cross sections for inner-shell ionization by light ions ranging from the classical to the quantal. Two of those which employ a quantal treatment for the target electron are the plane-wave Born approximation (PWBA)[14] and the semiclassical approximation (SCA).[15] The SCA, in which the motion of the projectile is treated classically with a prescribed trajectory, provides the ionization probability as a function of impact parameter. It is equivalent to the PWBA for the total cross section for a straight-line trajectory in the limit of projectile energy loss small compared to its initial energy.

The PWBA is found to be fairly successful in predicting total cross sections for high or even moderate projectile velocities (projectile velocity $\gtrsim$ target electron velocity), but at lower velocities discrepancies of one or two orders of magnitude occur. These have been explained[4,16,17] in large part by a number of specific physical phenomena that occur during the ionization process. The most important of these is the binding effect, the change in the binding energy of the target electron from the presence of the charged projectile. Changes in the binding energy are important because of the dependence of the total cross section on this quantity which becomes stronger as the projectile velocity decreases. Quantitative estimates of this effect have been made by evaluating the binding energy of the target electron in the presence of the projectile fixed at some effective distance from the target nucleus.

Other effects which become increasingly significant at lower projectile velocities include the retardation and deflection of the projectile on a

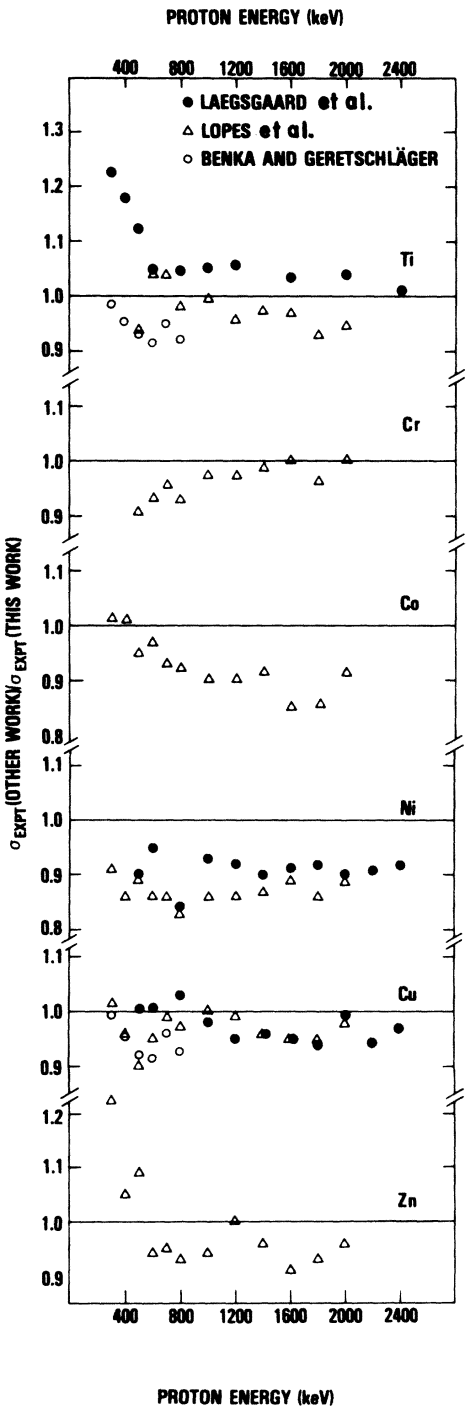

FIG. 2. Ratio of some recent measurements to the present measurements as a function of proton energy for the proton-induced total K-shell ionization cross section in six target materials. Data have been plotted as ratios in order to illustrate best their differences over the entire proton energy range.

Coulomb trajectory, as opposed to a straight-line constant-velocity path, the effect of the energy loss of the projectile during interaction, and the effects of relativity on the motion of the target electron. At moderate velocities the change in the electron wave function arising from the polarized distortion induced by the projectile (polarization effect) is important. These effects have been estimated in different ways by different authors[4,16,17] and have been incorporated into both the PWBA and the SCA to remove much of the discrepancy between theory and experiment at low velocities.

A systematic approach for going beyond the usual Born approximation but still within the context of perturbation theory is provided by perturbed-stationary-state (PSS) theory.[6] In this approach, which is framed within the SCA, the electron wave function is expanded in terms of basis states which form exact solutions to the total Hamiltonian, target electron plus interaction with the projectile, at each instant of time or, equivalently, for each position of the projectile along its trajectory. Thus, the electron is assumed to respond instantaneously to the motion of the projectile. This is the adiabatic approximation. PSS theory includes both binding and Coulomb trajectory effects in a natural way and has been used to justify the treatment of the binding effect when incorporated into the PWBA.

Land *et al.*[5] have described an approach implementing PSS theory to calculate the impact-parameter dependence of K-shell ionization from which the total cross section is obtained. These calculations have been performed in an approximation (PSS/1) in which the Coulomb trajectory of the projectile is replaced by an equivalent straight-line trajectory. For each physical impact parameter, this trajectory is characterized by an effective impact parameter, incident velocity and electron binding energy, and by effective wave functions for the electron (wave-function relaxation). Each of these quantities is evaluated at the distance of closest approach of the projectile to the target nucleus, except for the velocity which is taken to be an appropriate average. The binding energy of the electron in the presence of the projectile is determined by minimizing the energy obtained from first-order perturbation theory with respect to an assumed ground-state wave function.[18] These calculations employ the Merzbacher-Lewis wave functions[14] to take account of outer screening. This differs from previous calculations[17] in the SCA in which unscreened hydrogenic wave functions are

used. The Slater prescription is used for inner screening. For the outgoing electron we keep up to d states, corresponding to keeping the quadrupole term in an expansion of the potential. We have also performed in a few instances calculations (PSS/C) for the total cross sections in which the probability amplitude is obtained by integrating along the exact Coulomb trajectory with the use of Hartree-Fock wave functions expressed in a basis system developed by Reading and co-workers.[19] Good agreement between the two approaches is obtained.[5] The agreement shows that PSS/1 constitutes an accurate implementation of PSS theory. We emphasize that these approaches require no parameters and that the total cross section is obtained directly from the impact-parameter dependence.

Results of our calculations for the total cross section (PSS/1) are described in Fig. 3 by displaying the ratio of our experimental measurements to the theoretical values. Binding and Coulomb trajectory effects occur automatically and the energy-loss and relativistic effects are included from the theoretical work of Brandt and Lapicki.[4] Results are shown with and without relativistic and energy-loss effects in order to illustrate their importance. The polarization effect is not considered. We note the general trend for the theoretical values to be too large at low energies and too small at higher energies. In particular, the theoretical results lie above the experimental data by about 10% at the lowest energies except for Ti for which the theoretical values lie about 20% too high. The difference at the higher energies is explained in large part by the absence in our calculations of the polarization effect, as preliminary calculations show. We have no detailed explanation for the difference at lower energies at the present time. There is some indication from calculations reported in the literature[20] that the use of realistic wave functions for the electron provides a reduction in values for the total cross section at lower energies from those predicted with hydrogenic wave functions, but this is not a firm conclusion at this time.[5] This observation may be relevant here even though the calculations shown above are based upon the Merzbacher-Lewis modification of hydrogenic wave functions which is superior to the use of unscreened hydrogen wave functions to describe the continuum.[21]

We have also performed calculations employing a theory based upon the PWBA in which all of the effects which influence inner-shell ionization listed

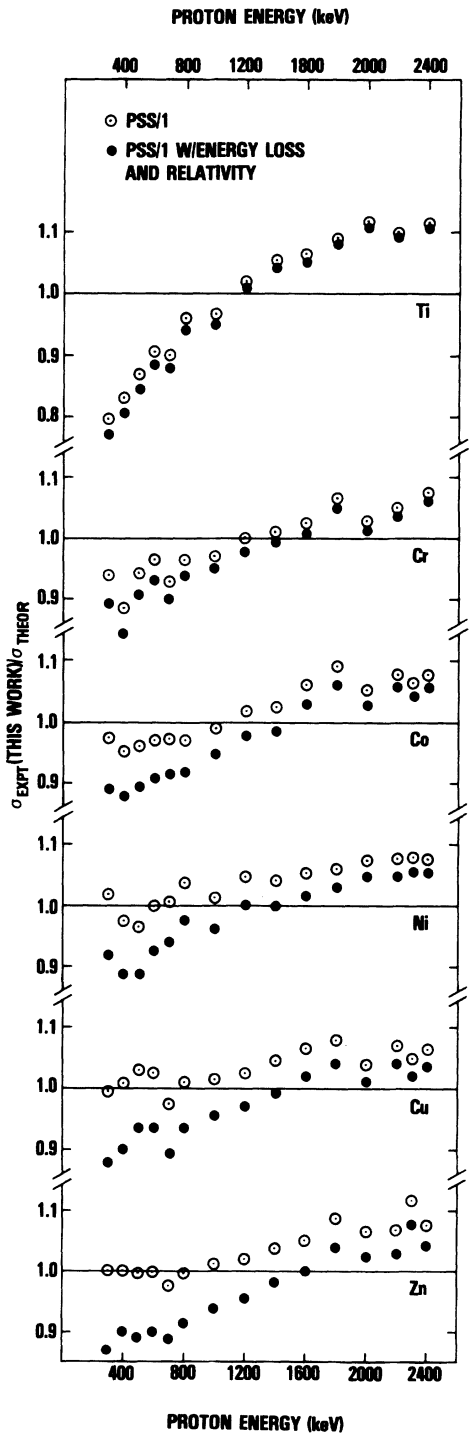

FIG. 3. Ratio of the present experimental measurements to the results of perturbed-stationary-state theory, PSS/1, and to the same results corrected for the effect of projectile energy loss and relativity as a function of proton energy. These corrections to PSS/1 are estimated on the basis of ECPSSR theory.

previously are included. This theory, designated by ECPSSR, has been developed by Brandt and Lapicki and co-workers.[4,16] As in Fig. 3, these results are expressed in terms of the ratio of our experimental values to the theoretical predictions and are shown in Fig. 4. Overall, very close agreement between this theory and our data is seen. In particular, for Co, Ni, Cu, and Zn the agreement is in almost every instance to within 3%. For Ti there is a trend for the theoretical values to lie about 10% above the data at the lowest energies, falling to about 3% above the highest.

We see that both PSS/1 and ECPSSR provide a close correlation with the experimental data, with ECPSSR being more accurate. Thus, ECPSSR offers good predictive capability, at least in the region discussed here. Both theories, PSS/1 and ECPSSR, employ the same physical principles as regards the treatment of the binding effect but PSS/1 is the more accurate formalism. No parameters are required in PSS/1, while two parameters related to the binding and polarization effects must be determined for ECPSSR.[4,16] While the polarization effect has not yet been considered in detail in PSS/1, its effect is to increase the calculated values for the total cross section by 1% or 2% at the lowest energies of interest here. We conclude that, since PSS/1 is an accurate implementation of the PSS formalism[6] and shows disagreement with the experimental data at low energies, first-order theories with hydrogenlike wave functions are deficient at low energies. The largest differences for both calculations, PSS/1 and ECPSSR, occur for Ti, the target having the smallest atomic number of those we have considered and thus the largest effective coupling. This may suggest the inadequacy of the perturbation approximation as employed in these theories. Furthermore, we note the need for more realistic wave functions for the electron.

Finally, we point out that, in the comparisons of our data with either set of theoretical results, there is no special trend for the Ni data when viewed along with the Cu or Zn data. This observation is in contrast with what we had previously noted in the comparisons of our data with that of the other experimental groups.

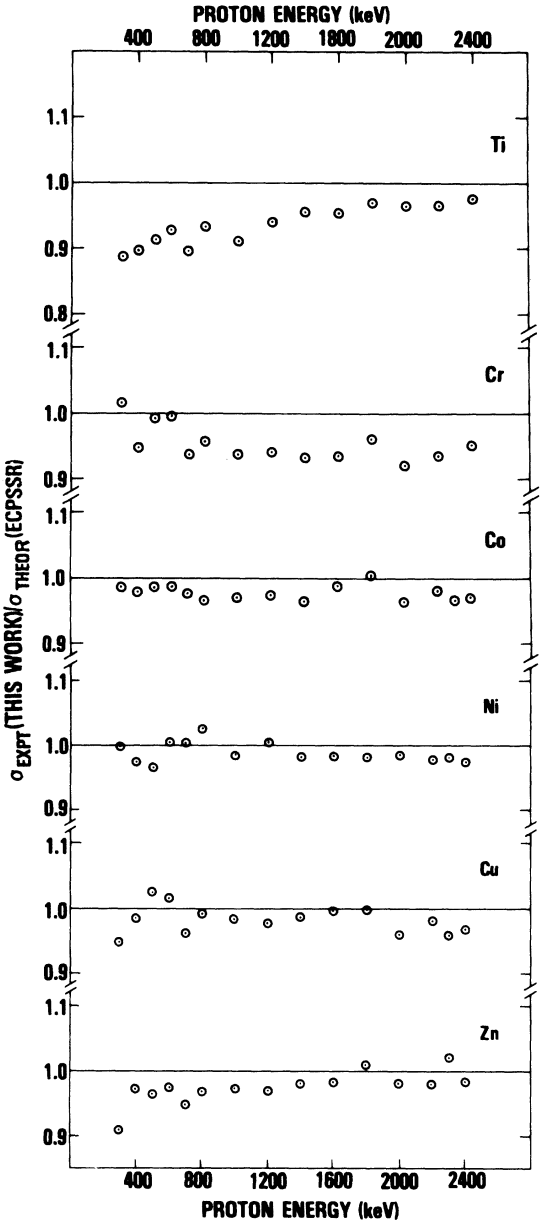

FIG. 4. Ratio of the present experimental measurements to the ECPSSR theoretical results as a function of energy for the proton-induced total K-shell ionization cross sections in Ti, Cr, Co, Ni, Cu, and Zn.

V. CONCLUSIONS

In this paper we present absolute K-shell vacancy-production cross sections for incident protons with energies in the range from 0.3 to 2.4 MeV in targets of Ti, Cr, Co, Ni, Cu, and Zn measured to high accuarcy ($\approx$5%). The agreement with the measurements reported by other investigations is generally to within the quoted errors, in the majority of cases to within 5%. The present measurements agree closely with the theoretical results for both formalisms considered here in detail, the ECPSSR theory to within 3% and the PSS/1 theory to within 10%. It is noted that for the

present experimental parameters, the cross sections range over four orders of magnitude.

There are several aspects in this study which remain puzzling. The first concerns the discrepancies for the experimental measurements at the lower proton energies. In particular, there is a systematic increase in the cross sections measured by others relative to our measurements, especially for Ti and Zn and somewhat for Co. However, for Cr the opposite is true. For Ni and Cu no trend exists. The second concerns the results for nickel. The measurements reported here are approximately 10% larger than those reported in two independent investigations. However, all three data sets agree very closely for copper which is the next larger atomic number. When our data are compared with either of the two theoretical formalisms, there is no special trend observed as the atomic number varies. In addition, our data follow a smoothly varying function of proton energy with little scatter in the experimental data for all the target elements investigated. The results for nickel could be explained if both of the other data sets had a systematic error of a few percent. Finally, we note that for titanium the largest differences between our data and both sets of theoretical calculations exist. We have no explanation for this at the present time.

The data presented here, along with other accurate measurements, provide increased confidence in the data base for the K-shell vacancy-production cross sections of these elements. However, there is a continuing need for accurate measurements for higher- and lower-z targets and for helium-ion beams. In addition, fundamental theoretical treatments which accurately account for the physical processes in a unified manner are required to understand more fully inner-shell ionization for light ions. In particular, the effect of nonadiabaticity on the response of the electron wave function to the intruding projectile requires study. Polarization effects, relativistic effects, and projectile energy loss need to be included in the PSS formalism.

ACKNOWLEDGMENTS

The authors wish to express their special thanks to Mr. P. K. Cady for his valuable assistance with both the data acquisition and analysis. It is also our pleasure to acknowledge Dr. J. M. R. Hutchinson of the National Bureau of Standards for his help in verifying the calibration accuracy of the radioactive sources used. Finally, we gratefully acknowledge the financial support of this Center's Independent Research Program and of the Office of Naval Research which made the study possible.

---

*Also at Catholic University of America, Washington, D. C. 20064.

[1]R. K. Gardner and T. J. Gray, At. Data Nucl. Data Tables 21, 515 (1978).

[2]E. Laegsgaard, J. U. Andersen, and F. Hogedel, Nucl. Instrum. Methods 169, 293 (1980).

[3]J. S. Lopes, A. P. Jesus, and S. C. Ramos, Nucl. Instrum. Methods 169, 311 (1980).

[4]W. Brandt and G. Lapicki, Phys. Rev. A 23, 1717 (1981).

[5]D. J. Land, M. D. Brown, D. G. Simons, and J. G. Brennan, Nucl. Instrum. Methods 192, 53 (1982).

[6]G. Basbas, W. Brandt, and R. H. Ritchie, Phys. Rev. A 7, 1971 (1973).

[7]W. Bambynek, B. Craseman, R. W. Fink, H. U. Freund, H. Mark, C. D. Swift, R. E. Price, and P. V. Rao, Rev. Mod. Phys. 44, 716 (1972).

[8]J. S. Lopes, A. P. Jesus, G. P. Ferreira, and F. B. Gil, J. Phys. B 11, 2181 (1978); S. R. Wilson, F. D. McDaniel, J. R. Rowe, and J. L. Duggan, Phys. Rev. A 16, 903 (1977); F. D. McDaniel, T. J. Gray, and R. K. Gardner, *ibid.* 11, 1607 (1975); T. J. Gray, R. Lear, R. J. Dexter, F. N. Schwettmann, and K. C. Wiemer, Thin Solid Films 19, 103 (1973); R. C. Bearse, D. A. Close, J. J. Malanify, and C. J. Umbarger, Phys. Rev. A 7, 1269 (1973).

[9]J. M. R. Hutchinson, Natl. Bur. Stand. (private communication).

[10]W. J. Veigele, At. Data 5, 51 (1973).

[11]G. G. Johnson, Jr. and E. W. White, ASTM Data Ser. DS 46, 1 (1970).

[12]J. F. Ziegler, *Helium Stopping Powers and Ranges* (Pergamon, New York, 1977).

[13]O. Benka and M. Geretschläger, J. Phys. B 13, 3223 (1980).

[14]E. Merzbacher and H. W. Lewis, in *Encyclopedia of Physics*, edited by S. Flügge (Springer, Berlin, 1958), Vol. 34, pp. 166 –192.

[15]J. Bang and J. M. Hansteen, K. Dan. Vidensk. Selsk., Mat.-Fys. Medd. 31, No. 13 (1959).

[16]G. Basbas, W. Brandt, and R. Laubert, Phys. Rev. A 7, 983 (1973); 17, 1655 (1978).

[17]E. Laegsgaard, J. U. Andersen, and M. Lund, *10th International Conference on Physics of Electronic and Atomic Collisions, Paris*, edited by G. Watel (North-Holland, Amsterdam, 1978), p. 353.

[18]W. Brandt, R. Laubert, and I. Sellin, Phys. Rev. 151, 56 (1966).

[19]A. L. Ford, E. Fitchard, and J. F. Reading, Phys. Rev. A 16, 133 (1977); G. L. Swafford, J. F. Reading, A. L. Ford, and E. Fitchard, *ibid.* 16, 1329 (1977).

[20]K. Aashamar and P. Amundsen, J. Phys. B 14, 483 (1981).

[21]O. Aashamar and L. Kocbach, J. Phys. B 10, 869 (1977).